Available online at www.sciencedirect.com
SCIENCE DIRECT
ELSEVIER
International Journal of Mass Spectrometry 249–250 (2006) 215–221
International Journal of Mass Spectrometry
www.elsevier.com/locate/ijms

Delayed neutral-atom evaporation of photoexcited anionic gold clusters

Alexander Herlert *, Lutz Schweikhard

Institut für Physik, Ernst-Moritz-Arndt-Universität, 17487 Greifswald, Germany

Received 10 November 2005; received in revised form 19 December 2005; accepted 19 December 2005
Available online 23 January 2006

Abstract

The technique of time-resolved photodissociation in a Penning trap has been extended from cationic to anionic metal clusters. As a proof of principle the size-selected gold clusters Au_{14}^- and Au_{17}^- have been investigated. Superposed on the expected exponential decrease (increase) of the intensity of the precursor (product) cluster ion an oscillation of the yield is observed. This oscillation, which has not been noticed in the case of cations, is attributed to the magnetron motion of the ions in the trap. Reaction-rate constants for the monomer evaporation have been determined. The dissociation energies deduced from the Weisskopf rate equation are compared to extrapolations from model-free dissociation energies of positively charged gold clusters.
© 2005 Elsevier B.V. All rights reserved.

Keywords: Penning trap; Metal cluster anions; Time-resolved photodissociation; Dissociation energy

1. Introduction

Clusters form an intermediate state of matter between isolated atoms and bulk material, where the properties do not necessarily scale with the cluster size, i.e., with the number of atoms or molecules of the cluster. On the contrary, some cluster properties show significant deviations from a smooth transition from large to small systems where each atom counts [1]. The binding energy of atoms to the cluster, i.e., the dissociation energy in the case of monomer evaporation, describes the stability of the cluster against disintegration after an excitation by collision with atoms, photoabsorption or electron interaction. The binding energy, like other parameters, is not a smooth function of the cluster size n, but exhibits large steps, which appear as corresponding characteristic ion yields in mass spectra both directly from cluster sources and after forced fragmentation of (size-selected) clusters.

A famous example are the abundance spectra of small sodium clusters, that showed not only an odd–even staggering but also large steps at cluster sizes $n = 8$, 20, 40, 58, 92 [2]. These were explained in the framework of the Jellium model [3]: the atomic valence electrons are bound in the mean-field potential of the ionic core and like in atomic physics they obey the Pauli principle and occupy different energy levels. Thus closed electronic shells lead to a higher stability, i.e., to larger ionization and atom-binding energy. Likewise geometric shells and especially stable structures have been found, e.g., for noble metal clusters [4].

Whereas in the case of geometric structures the charge state z of the cluster may be of minor importance, electronic shells depend directly on the number of electrons, i.e., the stable cluster sizes are a function of both n and z. Thus to distinguish electronic and geometric effects, the investigation of the cluster properties is required not only as a function of size but also as a function of charge state. For highly positively charged monovalent metal clusters the dependence on the number of valence electrons has been observed [5–8]. In this work, the extension of the method of time-resolved photodissociation in a Penning trap [9] is shown for negatively charged gold clusters in order to test its feasibility.

2. Experimental set-up and procedure

The measurements have been performed with the Cluster-Trap set-up which employs a Penning trap for the storage, size-selection and investigation of cluster ions. An overview and details of the experimental procedures can be found in [10]. In Fig. 1 a sketch of the main devices and sections is shown. The cluster anions are produced in a laser vaporization source (along with cations and neutral species) and transferred via ion optical

* Corresponding author at: CERN, Physics Department, 1211 Geneva 23, Switzerland.
E-mail address: alexander.herlert@cern.ch (A. Herlert).

1387-3806/$ – see front matter © 2005 Elsevier B.V. All rights reserved.
doi:10.1016/j.ijms.2005.12.027

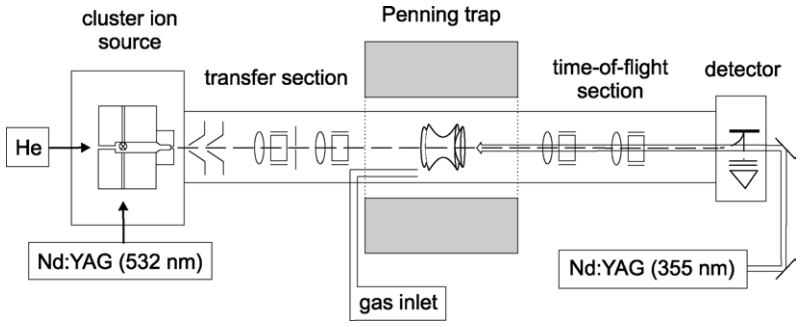

Fig. 1. Sketch of the experimental set-up of ClusterTrap as used for the present investigations. For the cluster production and excitation the same Nd:YAG laser has been applied with the second and third harmonic, respectively.

elements into a Penning trap where they are captured in flight. The Penning trap is located in a vacuum tube inside a superconducting magnet ($B = 5$ T). The ions perform oscillatory motions in the crossed static electric and magnetic fields, a superposition of three independent modes: the cyclotron, the magnetron, and the axial (trapping) motion [11]. For the present experiments the cluster size of interest is selected by removing the unwanted ions from the trap by increasing the radius of their radial cyclotron motion with a dipolar radiofrequency (rf) excitation.

After centering of the size-selected anions in the middle of the trap by use of a buffer-gas assisted quadrupolar rf-excitation [12], the clusters are subjected to a pulse (∼10 ns) of a frequency-tripled Nd:YAG laser ($E_{ph} = 3.49$ eV). The FWHM of the laser profile was about 8 mm while the cluster ion cloud has usually a width of about 1 mm after the buffer-gas centering [13]. Thus all ions experience almost the same fluence. In the present investigation the laser fluence was also kept low deliberately to avoid extensive multi-photon absorption (see below).

In order to observe the decay process time-resolved, the time between photoexcitation and analysis of the surviving precursors as well as the fragments produced (axial ejection of the anions and time-of-flight (TOF) mass spectrometry) can be varied between 10 μs and up to several hundred milliseconds. The Daly-type micro-channel-plate detector has single-ion detection capability and allows to monitor the ion yield as a function of cluster size. About 20 anions are observed in each measurement sequence of ion production, capture, storage/interaction, and detection. In order to obtain a statistically significant number of events, the sequence is repeated 50–100 times.

As mentioned above, the relative abundance of the precursor and the product cluster is measured as a function of the delay between irradiation and ejection. The expected behavior is demonstrated in Fig. 2(a): 20% of the precursor clusters are assumed to dissociate with a rate of $k = 10^3\ s^{-1}$. Since 70% of the clusters have not absorbed enough photons to undergo a decay, a plot with a logarithmic time scale is advantageous. In principle, the shape of the curve stays the same and only its position relative to the time axis changes. The relative abundance is given by

$$R_i(t) = \frac{N_i(t)}{N_0(t) + N_1(t)}, \quad i = 0, 1, \tag{1}$$

where $N_0(t)$ and $N_1(t)$ are the numbers of recorded precursor and product clusters which are described by

$$N_0(t) = N_{0,0} + N_{0,1}(e^{-kt} - 1) - N_{0,2}, \tag{2}$$

$$N_1(t) = N_{0,0} - N_0(t) = N_{0,1}(1 - e^{-kt}) + N_{0,2}. \tag{3}$$

$N_{0,0}$ is the number of initially stored precursor clusters, $N_{0,1}$ the initial number of precursor clusters that are observed to dissociate delayed into the product cluster, and $N_{0,2}$ denotes the number of precursor clusters that decay faster than the experimental time scale, e.g., due to multi-photon absorption, and that appear as an offset in the plot. In the example of Fig. 2(a), the relative yield for fast and time-resolved decay is 10% and 20%, respectively.

The normalization in Eq. (1) reduces the effect of fluctuations of the cluster production in the laser vaporization source. In order to also take care of drifts in the dissociation-laser intensity, a further normalization is performed, where a second experimental cycle with a fixed delay time t_0 (which is much larger than the life-time $1/k$) is performed in alternation to the cycle with a varied delay time. The "normalized relative abundance" then becomes:

$$R'_i(t) = \frac{R_i(t)}{R_i(t_0)} = \frac{N_i(t)}{N_0(t) + N_1(t)} \times \left[\frac{N_i(t = t_0)}{N_0(t_0) + N_1(t_0)}\right]^{-1}, \quad i = 0,\ 1. \tag{4}$$

$t_0 = 100$ ms is the fixed delay time of the example shown in Fig. 2(b). Note that by definition both normalized relative abundances R'_0 and R'_1 are equal to 1 as the time t_0 is approached. For $t = 0$ and $t_0 = \infty$ the normalized relative abundances are

$$R'_0(0) = \frac{N_{0,0} - N_{0,2}}{N_{0,0} - N_{0,1} - N_{0,2}}, \tag{5}$$

$$R'_1(0) = \frac{N_{0,2}}{N_{0,1} + N_{0,2}}, \tag{6}$$

which give, when experimentally determined, the relative abundances of clusters with a time-resolved decay:

$$\frac{N_{0,1}}{N_{0,0}} = \frac{(1 - R'_1(0))(R'_0(0) - 1)}{R'_0(0) - R'_1(0)} \tag{7}$$

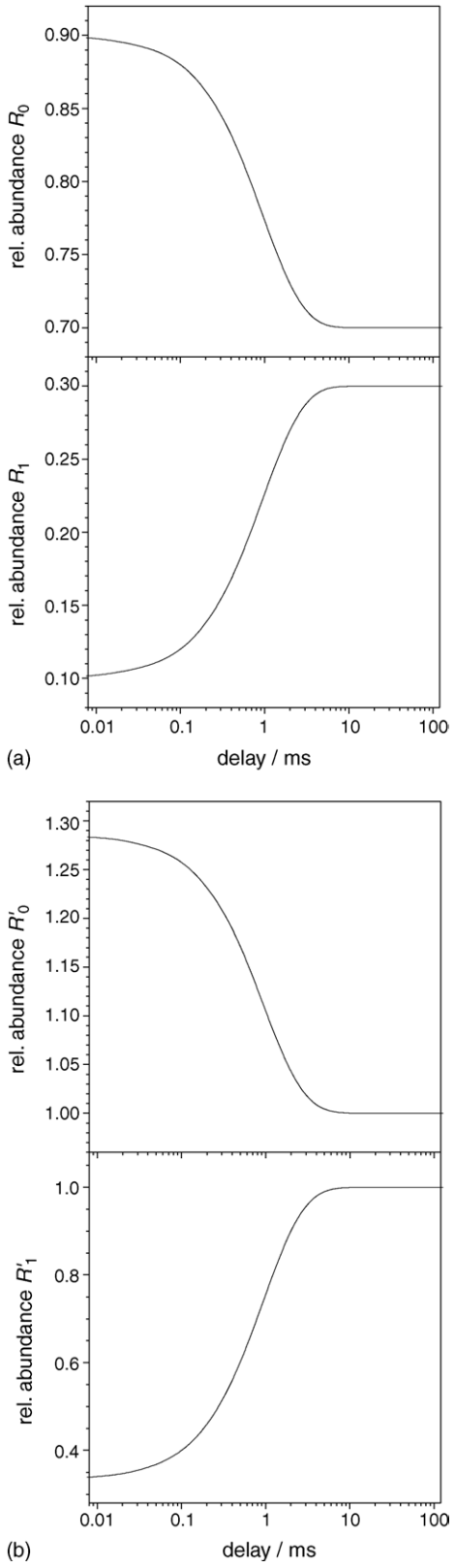

Fig. 2. Demonstration of the relative abundance R_0 and R_1 (a) and "normalized relative abundance" R'_0 and R'_1 (b, see text) of the precursor and the product cluster as a function of the delay between photoexcitation and ejection for mass analysis. The solid lines are theoretical curves for decay rates of $k = 10^3\ s^{-1}$ with a time-resolved decay and fast decay for 20% and 10% of the precursor clusters, respectively.

and a fast decay:

$$\frac{N_{0,2}}{N_{0,0}} = R'_1(0)\frac{R'_0(0) - 1}{R'_0(0) - R'_1(0)}. \quad (8)$$

In addition to dissociation, the emission of an electron from the photoexcited cluster anion may occur. The branching ratio for electron emission versus neutral-atom evaporation is strongly depending on the element under consideration and the cluster sizes investigated. This has been observed in experiments on photoexcitation of small silver and gold-cluster anions [14,15] and in the study of photoexcitation of dianionic gold-clusters as a function of cluster size [16].

With the present approach electron emission cannot be observed. However, in an independent experiment, where two cycles were alternated with the laser enabled in the first and disabled in the second one, no significant ion loss was observed for delay times up to 100 ms. Electron emission will thus not be considered in the following.

3. Results

As an example for delayed photodissociation of gold cluster anions, the sizes Au_{14}^- and Au_{17}^- have been studied. The

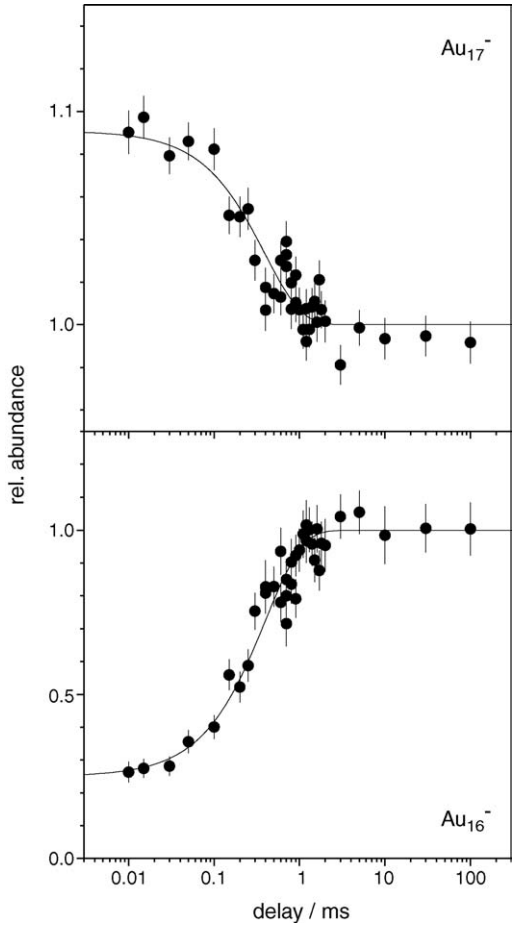

Fig. 3. Normalized relative abundance of Au_{17}^- and Au_{16}^- as a function of the delay time between photoexcitation and ejection for mass analysis. The lines are fits of Eq. (4) to the data points.

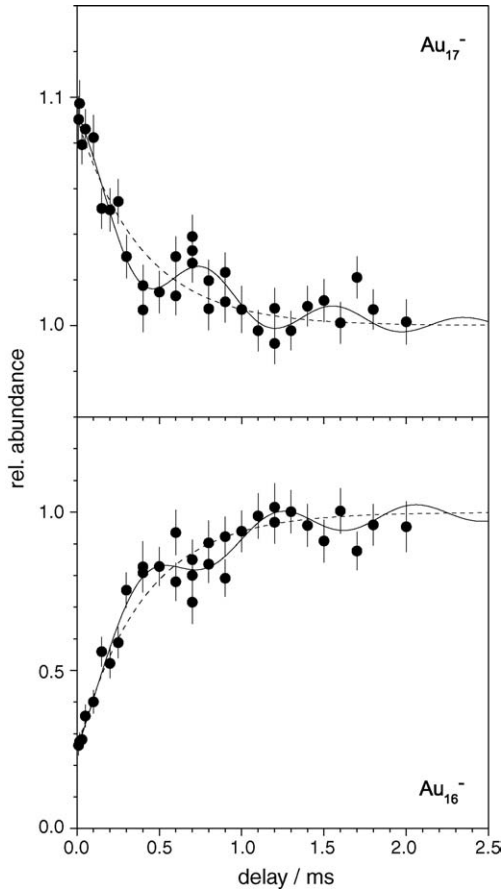

Fig. 4. Normalized relative abundance of Au_{17}^- and Au_{16}^- as a function of the delay time between photoexcitation and ejection for mass analysis plotted with a linear time scale. The solid lines are fits of Eq. (9) to the data points. The dashed lines show only the exponential behavior.

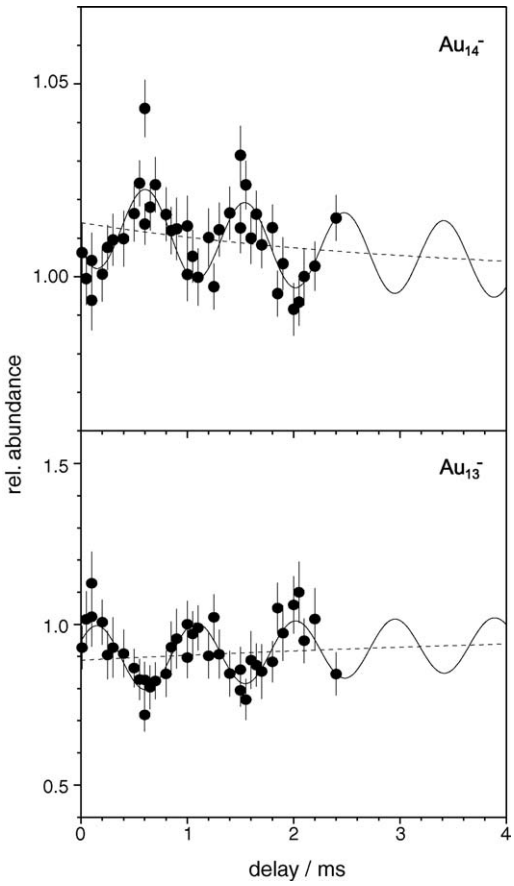

Fig. 5. Normalized relative abundance of Au_{14}^- and Au_{13}^- as a function of the delay time between photoexcitation and ejection for mass analysis plotted with a linear time scale. The solid lines are fits of Eq. (9) to the data points. The dashed lines show only the exponential behavior.

normalized relative abundance of Au_{17}^- and its product Au_{16}^- is plotted as a function of the delay between laser irradiation and TOF mass analysis in Fig. 3. The fit of Eq. (4) to the data points yields decay constants $\tau_{17} = 1/k_{17} = 0.39(4)$ ms and $\tau_{16} = 0.40(3)$ ms.

Plotting the data points with a linear time scale as shown in Fig. 4 they exhibit an oscillation in addition to the exponential decay. This can be described by

$$r = c_1 + c_2\,e^{-kt} + c_3\,e^{-\gamma t}\sin(\omega t + \phi), \qquad (9)$$

where ω is the oscillation (angular) frequency, γ the damping of the oscillation and ϕ is the phase of the oscillation at $t = 0$. With this approach a fit yields the decay constants $\tau_{17} = 0.49(7)$ ms and $\tau_{16} = 0.46(4)$ ms, which are slightly larger than those from a fit without oscillation. The oscillation has a frequency $\omega_{17}/2\pi = 1274(92)$ Hz and $\omega_{16}/2\pi = 1211(92)$ Hz, a phase of $\phi_{17} = 84(23)^\circ$ and $\phi_{16} = 92(24)^\circ + 180^\circ$, and a damping of $\gamma_{17} = 810(550)\,s^{-1}$ and $\gamma_{16} = 500(600)\,s^{-1}$. Thus the data are consistent with no damping of the oscillation on the time scale of the present experiment.

In the case of Au_{14}^- (see Fig. 5) the oscillation is much more pronounced as compared to the exponential behavior. A fit of Eq. (9) gives the decay constants $\tau_{14} = 3.2(1.8)$ ms and $\tau_{13} = 6.7(6.4)$ ms, the frequencies $\omega_{14}/2\pi = 1070(37)$ Hz and $\omega_{13}/2\pi = 1069(35)$ Hz, and the phases $\phi_{14} = -146(18)^\circ$ and $\phi_{13} = -146(16)^\circ + 180^\circ$. Again, no damping of the oscillation could be determined from the data.

By increasing the focussing of the laser beam a higher fluence was achieved (the FWHM was about 4 mm). It led to the absorption of further photons by Au_{14}^- and thus to a sequential decay to Au_{12}^- (see Fig. 6). Note that the evaporation of a neutral dimer is not expected in the case of Au_{14}^- but may occur for Au_{13}^- [17]. In addition, the oscillation amplitude is larger than in the case of less focussing. However, the fitted frequencies $\omega/2\pi = 1062(18)$ Hz, $\omega/2\pi = 1067(20)$ Hz, and $\omega/2\pi = 1062(22)$ Hz for Au_n^-, $n = 14$, 13, 12, respectively, and the phases $\phi_{14} = -151(9)^\circ$, $\phi_{13} = -162(10)^\circ + 180^\circ$, and $\phi_{12} = -141(11)^\circ + 180^\circ$ are similar as for the decay $Au_{14}^- \rightarrow Au_{13}^-$ at low fluence.

In all cases an offset of the relative product yield is observed. The application of Eqs. (7) and (8) to the fitted relative abundance at $t = 0$ as shown in Figs. 4 and 5 yields a fraction of 8% of time-resolved Au_{17}^- decays and a fraction of 2.7% with a fast decay (where more than two photons have been absorbed). For Au_{14}^- only 1.2% of the precursor cluster anions are observed to decay delayed whereas about 10% exhibit a fast decay (absorption of more than one photon).

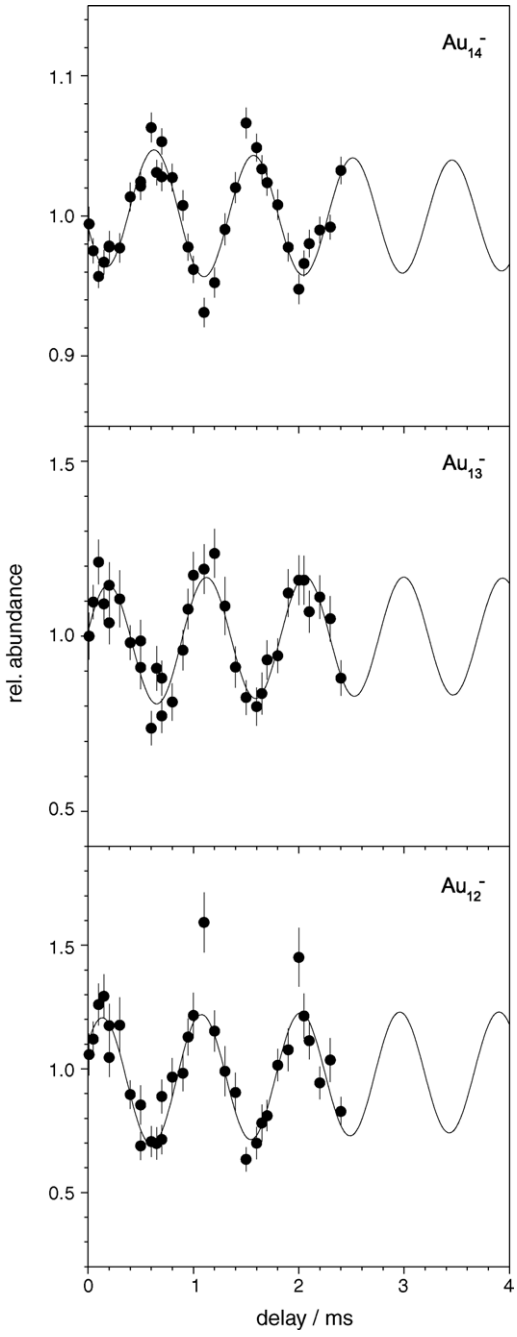

Fig. 6. Normalized relative abundance of Au_{14}^-, Au_{13}^-, and Au_{12}^- as a function of the delay time between photoexcitation and ejection for mass analysis in the case of a more focussed laser beam. The solid lines are fits of Eq. (9) to the data points.

4. Discussion

4.1. Oscillation of ion yield

In all investigated cases an oscillation of the ion yield is observed. This oscillation is in phase with the photoexcitation with no damping in the millisecond time range. The frequency of this oscillation is close to the expected magnetron frequency of the cluster anions, e.g., 991 Hz for Au_{14}^- calculated from the trap parameters: magnetic field $B = 5$ T, potential between ring and endcap electrodes $U_0 = 12$ V, and trap dimension $d_0^2 = 200\,\mathrm{mm}^2$ [11]. This suggests, that the ions have gained a magnetron radius after the excitation and that their center of rotation is not aligned with the experimental axis. The origin of this coherent motion is not clear. In case of experiments with positively charged clusters no such oscillation has been observed. One difference between the storage of positively and negatively charged ions is that in the latter case electrons can be trapped simultaneously with the cluster anions. This may create a space charge due to laser irradiation which can influence the trapping potential of the ions and thus their ion motion in the trap. It would explain the increased value of the magnetron frequency [18,19]. However, as long as the ion distribution is symmetric with respect to the trap axis there is no obvious reason for the observed behavior. In addition, the symmetry breaking seems to depend on the role of the species in the decay process: precursors and fragments are observed to move in opposite phases. However, sequential decay does not lead to any additional phase shift: in the case of the decay of Au_{14}^- the products Au_{13}^- and Au_{12}^- show the same phase.

4.2. Decay rates

Although the origin of the oscillation is not clear, it can be taken into account in the fit of the exponential decay (or growth) of the ion yield in order to extract the relevant decay rate as shown above. In the following the experimental rates will be compared to a decay-rate model to deduce the dissociation energy of the cluster anions. As in previous investigations [20] the Weisskopf rate equation is applied. It is given by [21]:

$$k(n, E) = \frac{g m_\mu}{\pi^2 \hbar^3} \sigma_{n-1} k_B^2 T_P^2 \frac{\rho_{n-1}(E - D)}{\rho_n(E)}, \tag{10}$$

where the degeneracy of the product (monomer) is $g = 2$, the reduced mass of the decay channel $m_\mu = (n-1)n^{-1}m_0$ (with m_0 mass of the gold atom), the capture cross-section of a gold atom:

$$\sigma_{n-1} = \pi r_0^2 ((n-1)^{1/3} + 1)^2 \tag{11}$$

with the Wigner–Seitz radius $r_0 = 1.59$ Å, the temperature of the product cluster $T_P = T_{n-1}(E - D)$, and the level densities ρ_{n-1} and ρ_n of the product and the precursor cluster, respectively. D is the dissociation energy to be determined.

The level densities are approximated by $k_B \ln(\rho) = S_n$ with the entropy of the cluster [22]:

$$S_n = \int \frac{1}{T_n(E)}\,\mathrm{d}E, \tag{12}$$

where the temperature is deduced from the energy–temperature relation

$$E(T) = n_{\mathrm{eff}} \int_0^T C(T')\,\mathrm{d}T' \tag{13}$$

with the effective number of atoms $n_{\mathrm{eff}} = (3n - 6)/3 = n - 2$. The heat capacities are taken from the gold bulk values [23] as shown

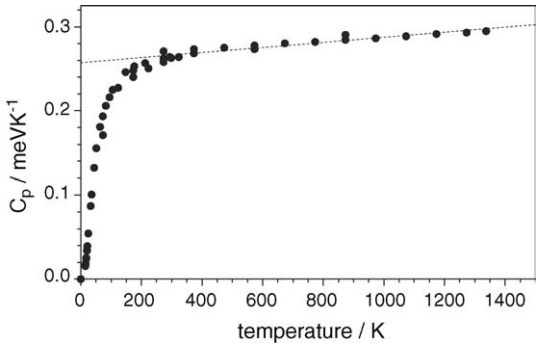

Fig. 7. Heat capacity of bulk gold as a function of the temperature. The dashed line shows a fit of Eq. (14) to the data points above $T = 230$ K.

in Fig. 7. For temperatures above $T = 230$ K a linear behavior of $C(T)$ is assumed:

$$C(T) = a_1 + 2a_2T \tag{14}$$

with the fitted parameters $a_1 = 0.257\,\text{meV K}^{-1}$ and $a_1 = 1.51 \times 10^{-5}\,\text{meV K}^{-2}$ (see dashed line in Fig. 7). The energy becomes

$$E(T) = n_{\text{eff}}(a_0 + a_1T + a_2T^2). \tag{15}$$

Matching Eqs. (13) and (15) for temperatures above $T = 230$ K yields the fit parameter $a_0 = -16.1$ meV. The temperature of a cluster can now be calculated by inversion of Eq. (15).

The decay rates calculated from Eq. (10), where the total excitation energy is $E = E_{\text{ph}} + E_{\text{th}}$ with the photon energies $E_{\text{ph}} = 3.49$ eV and 2×3.49 eV for Au_{14}^- and Au_{17}^-, respectively, and the thermal energy $E_{\text{th}} = E(300\,\text{K})$, is matched to the experimental decay rates $k = 1/\tau$ by varying the dissociation energy D. The resulting dissociation energies are $D_{14} = 2.57(4)$ eV and $D_{17} = 3.80(1)$ eV, where only the statistical uncertainty is given. These error bars are quite small since the relation between the energy and the rate is exponential.

The two dissociation energies are plotted as a function of the cluster size in Fig. 8 (bottom, full symbols). For comparison the dissociation energies of anionic gold clusters as determined with the Born–Haber cycle are shown, too (open circles). To this end experimental values for the ionization potentials IP [24] and electron affinities EA [25] as well as the model-free dissociation energies for the singly positively charged gold clusters D_n^+ [26] (see Fig. 8, top) have been applied:

$$\begin{array}{ccccc} X_n^- & \xrightarrow{EA_n} & X_n & \xrightarrow{IP_n} & X_n^+ \\ \downarrow D_n^- & & \downarrow D_n & & \downarrow D_n^+ \\ X_{n-1}^- + X & \xrightarrow{EA_{n-1}} & X_{n-1} + X & \xrightarrow{IP_{n-1}} & X_{n-1}^+ + X \end{array} \tag{16}$$

and thus the dissociation energy for the anionic clusters is given by

$$D_n^- = EA_n - EA_{n-1} + IP_n - IP_{n-1} + D_n^+. \tag{17}$$

Since no uncertainties are given for the IP and EA values, an estimate of $\Delta IP = \Delta EA = 0.1$ eV is used for the calculation.

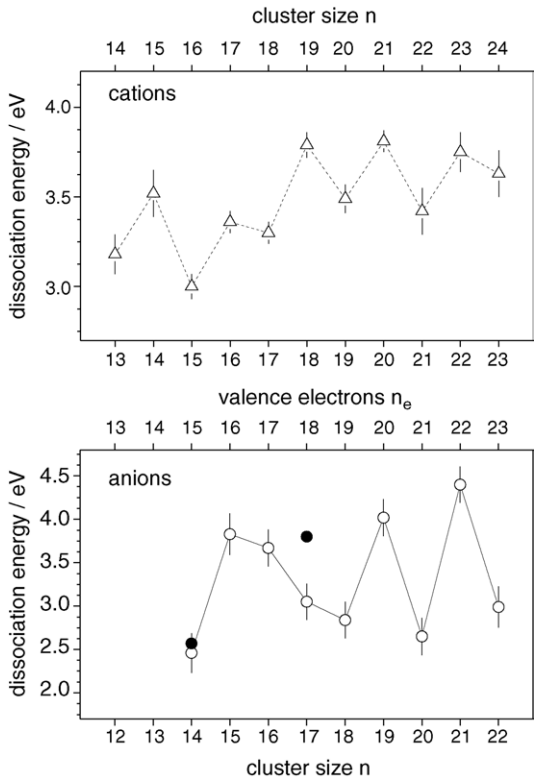

Fig. 8. Model-free dissociation energies of gold cluster cations (top, from [26]) and dissociation energies of gold cluster anions from Eq. (17) (bottom) as a function of the number of valence electrons n_e and the cluster size n. The full symbols represent the values from the present investigation.

The two values from the present work show a match in the case of $n = 14$ and a discrepancy in the case of $n = 17$. However, the dissociation energies calculated with the Born–Haber cycle are deduced from five experimental values, where four have unknown uncertainties. Thus significant deviations cannot be ruled out. The same conclusion applies for the increased amplitude of the odd–even-staggering as compared to the dissociation energy of the cations. If the model-free dissociation energies D_n^+ and the calculated energies D_n^- are both plotted as a function of the valence electrons as indicated in Fig. 8, a larger value for D_n^- at $n_e = 18$ might be expected, i.e., an electronic subshell closure.

5. Summary and outlook

Singly charged size-selected gold cluster anions have been stored in a Penning trap and were subjected to a laser pulse at a photon energy of $E_{\text{ph}} = 3.49$ eV. The monomer evaporation is time dependent as monitored by varying the delay between photoexcitation and ejection for mass analysis. In addition to the expected exponential decay, the ion yield shows an oscillation, which has a frequency in the order of but somewhat higher than the expected frequency of the magnetron motion of the stored ions. The origin of this oscillation is not yet understood and further investigations are required.

Nevertheless, from the observed exponential decrease of the relative ion abundance decay rates can be deduced. An evaluation in the framework of the Weisskopf decay-rate equation

yields dissociation energies for the cluster anions Au_{14}^- and Au_{17}^-. These have been compared to extrapolated model-free dissociation energies from cationic gold clusters. While this comparison gives no conclusive result, the present investigation is a proof of principle for the extension of the time-resolved photodissociation to anionic clusters. However, the observed ion yield oscillation limits its application. Further studies are required to find a conclusive explanation for the yield oscillations and to determine the dissociation energies of the full range of anionic gold clusters for an extensive comparison with their cationic counterparts.

Acknowledgements

This work has been supported by the Deutsche Forschungsgemeinschaft (DFG) under contract no. SCH401/13-3 and the Collaborative Research Centre SFB652 and the European Union (network on cluster cooling) under contract no. IHP-CT-2000-00026.

References

[1] W.A. de Heer, Rev. Mod. Phys. 65 (1993) 611.
[2] W.D. Knight, K. Clemenger, W.A. de Heer, W.A. Saunders, M.Y. Chou, M.L. Cohen, Phys. Rev. Lett. 52 (1984) 2141.
[3] M. Brack, Rev. Mod. Phys. 65 (1993) 677.
[4] O. Echt, K. Sattler, E. Recknagel, Phys. Rev. Lett. 47 (1981) 1121.
[5] I. Rabin, C. Jackschath, W. Schulze, Z. Phys. Chem. (Neue Folge) 169 (1990) 93.
[6] I. Rabin, C. Jackschath, W. Schulze, Z. Phys. D 19 (1991) 153.
[7] S. Krückeberg, G. Dietrich, K. Lützenkirchen, L. Schweikhard, C. Walter, J. Ziegler, Eur. Phys. J. D 9 (1999) 169.
[8] A. Herlert, S. Krückeberg, L. Schweikhard, M. Vogel, C. Walther, J. Electron Spectrosc. Relat. Phenom. 106 (2000) 179.
[9] U. Hild, G. Dietrich, S. Krückeberg, M. Lindinger, K. Lützenkirchen, L. Schweikhard, C. Walther, J. Ziegler, Phys. Rev. A 57 (1998) 2786.
[10] L. Schweikhard, K. Hansen, A. Herlert, G. Marx, M. Vogel, Eur. Phys. J. D 24 (2003) 137.
[11] L.S. Brown, G. Gabrielse, Rev. Mod. Phys. 58 (1986) 233.
[12] G. Savard, St. Becker, G. Bollen, H.-J. Kluge, R.B. Moore, Th. Otto, L. Schweikhard, H. Stolzenberg, U. Wiess, Phys. Lett. A 158 (1991) 247.
[13] C. Walther, St. Becker, G. Dietrich, H.-J. Kluge, M. Lindinger, K. Lützenkirchen, L. Schweikhard, J. Ziegler, Z. Phys. D 38 (1996) 51.
[14] Y. Shi, V.A. Spasov, K.M. Ervin, J. Chem. Phys. 111 (1999) 938.
[15] V.A. Spasov, Y. Shi, K.M. Ervin, Chem. Phys. 262 (2000) 75.
[16] L. Schweikhard, K. Hansen, A. Herlert, M.D. Herráiz Lablanca, G. Marx, M. Vogel, Int. J. Mass Spectrom. 219 (2002) 363.
[17] M. Vogel, K. Hansen, A. Herlert, L. Schweikhard, Eur. Phys. J. D 16 (2001) 73.
[18] J.B. Jeffries, S.E. Barlow, G.H. Dunn, Int. J. Mass Spectrom. Ion Processes 54 (1983) 169.
[19] L. Schweikhard, A. Herlert, G. Marx, in: M. Schauer, T. Mitchell, R. Nebel (Eds.), AIP Conference Proceedings on Non-neutral Plasma Physics V, vol. 692, 2003, p. 203.
[20] C. Walther, G. Dietrich, W. Dostal, K. Hansen, S. Krückeberg, K. Lützenkirchen, L. Schweikhard, Phys. Rev. Lett. 83 (1999) 3816.
[21] K. Hansen, U. Näher, Phys. Rev. A 60 (1999) 1240.
[22] V. Weisskopf, Phys. Rev. 52 (1937) 295.
[23] Gmelins Handbuch der anorganischen Chemie, 8, Aufiage, Gmelin-Institut fur anorganische Chemie (Hrsg.), Verlag Chemie GmbH, Weinheim/Bergstrasse, 1954.
[24] C. Jackschath, I. Rabin, W. Schulze, Z. Phys. D 22 (1992) 517.
[25] K.J. Taylor, C.L. Pettiette-Hall, O. Cheshnovsky, R.E. Smalley, J. Chem. Phys. 96 (1992) 3319.
[26] M. Vogel, K. Hansen, A. Herlert, L. Schweikhard, Phys. Rev. Lett. 87 (2001) 013401.